Quantitative understanding of molecular competition as a hidden layer of gene regulatory network

Ye Yuan[1,5], Lei Wei[1,5], Tao Hu[1], Shuailin Li[1], Tianrun Cheng[1], Jinzhi Lei[2], Zhen Xie[1], Michael Q. Zhang[1,3,4], Xiaowo Wang[1,*]

[1] Ministry of Education Key Laboratory of Bioinformatics, Center for Synthetic and Systems Biology, Department of Automation, Tsinghua University, Beijing, 100084, China

[2] Zhou Pei-Yuan Center for Applied Mathematics, Tsinghua University, Beijing, 100084, China

[3] Department of Basic Medical Sciences, School of Medicine, Tsinghua University, Beijing 100084, China

[4] Department of Biological Sciences, Center for Systems Biology, The University of Texas, Richardson, TX 75080-3021, USA

[5] These authors contributed equally to this work

[*] Correspondence: xwwang@tsinghua.edu.cn

Abstract

Molecular competition is ubiquitous, essential and multifunctional throughout diverse biological processes. Competition brings about trade-offs of shared limited resources among the cellular components, and it thus introduce a hidden layer of regulatory mechanism by connecting components even without direct physical interactions. By abstracting the analogous competition mechanism behind diverse molecular systems, we built a unified coarse-grained competition motif model to systematically compare experimental evidences in these processes and analyzed general properties shared behind them. We could predict in what molecular environments competition would reveal threshold behavior or display a negative linear dependence. We quantified how

competition can shape regulator-target dose-response curve, modulate dynamic response speed, control target expression noise, and introduce correlated fluctuations between targets. This work uncovered the complexity and generality of molecular competition effect, which might act as a hidden regulatory mechanism with multiple functions throughout biological networks in both natural and synthetic systems.

Keywords

systems biology, computational modelling, molecular competition regulation, synthetic biology, network motif

Introduction

Competition for limited resources matters at all scales of biology. Competition among different species can alter population distributions and ecological niches (Connell, 1983; Hardin, 1960; Schoener, 1983). Competition among individuals of the same species may slow down the growth rates of all competitors, driving natural selection and evolution (Bolnick, 2004; Svanback & Bolnick, 2007; Zwietering et al., 1990). Competition among adjacent cells in an organism can regulate their growth and viability, and enhance the dominance of cells with better fitness (Chang et al., 2015; Johnston, 2009; Khare & Shaulsky, 2006; Laird, 1964). In a microscopic scale, biological molecules within cells also face competition. Competition brings about trade-offs of shared limited resources among the cellular components (Hui et al., 2015; Scott et al., 2010; Weisse et al., 2015), and it thus introduces a hidden layer of regulatory mechanism by connecting components even without direct physical interactions. Miscellaneous phenomena caused by molecular competition have been reported in a variety of biological processes in diverse organisms. For example, DNA binding sites on plasmids can compete for transcription factor (TF) LacI to dictate its target gene expression in *E. coli* (Brewster et al., 2014). Noncoding RNAs transcribed from enhancer or promoter region can competitively bind to TF Yin-Yang 1 to trap the TF locally thus maintain gene expression stability in mouse embryonic stem cells (Sigova et al., 2015). mRNA, long-noncoding RNA and circular RNA molecules can competitively bind to microRNAs (miRNAs) to regulate various processes, such as cell

growth (Zheng et al., 2016), cell differentiation (Cesana et al., 2011) and tumor suppression (Sumazin et al., 2011). Competition between RNA binding proteins PGL-3 and MEX-5 for mRNA drives polar positioning of phase-separated liquid compartments in *C. elegans* embryos (Saha et al., 2016). Furthermore, competition effects are especially important in synthetic gene circuits. Every synthetic gene inevitably competes for common resources with each other in circuits and with endogenous biological processes, introducing unexpected circuit failures or host metabolic burdens (Cardinale & Arkin, 2012; Qian et al., 2017; Wu et al., 2016). In addition, when one genetic element drives two or more downstream elements, competition will modulate the dynamics of signal transduction (Jayanthi et al., 2013; Jiang et al., 2011). As a result, characteristics of each single component are insufficient for the accurate prediction of the whole circuit behavior, posing a serious obstacle in synthetic circuit design and application.

Several mathematical frameworks and synthetic gene experiments have been built to quantitatively understand the diverse biological phenomena caused by competition. For example, a thermodynamic model was used to explain the TF titration effect in *E. coli* (Brewster et al., 2014). Kinetic model has been adopted to analyze competing endogenous RNA (ceRNA) regulation (Ala et al., 2013), and we further quantified the ceRNA effect through synthetic gene circuits in human cell line (Yuan et al., 2015). A minimal model based on delay differential equations was established to describe ribosome allocation between endogenous and synthetic genes in *E. coli* (Gorochowski

et al., 2016). Queueing theory was introduced to describe the protein degradation process in *E. coli*, where target proteins as queues compete for degradation machine ClpXP as server (Cookson et al., 2011; Mather et al., 2010). However, common properties and underlying competition mechanisms in essence behind these diverse phenomena have not been systematically analyzed yet.

Here we propose that regulations by competition are ubiquitous, essential and multifunctional through diverse biological regulatory processes. By abstracting the analogous competition motif shared by diverse molecular systems, we built a unified coarse-grained kinetic model to systematically integrate experimental evidences in diverse biological processes and analyze the common properties shared among them. We organized these properties from steady-state behavior to dynamic responses, to quantify how competition could introduce constraints and indirect regulations among the targets and how the existence of competitors might influence regulator-target response characteristics. This work demonstrated the complexity and generality of the molecular competition effect, which is a ubiquitous hidden regulatory mechanism with diverse functions throughout different biological processes in both natural and synthetic life systems.

Results

A unified coarse-gained competition motif model

A number of phenomena caused by molecular competition have been reported in diverse biological systems recently (Brewster et al., 2014; Saha et al., 2016; Sigova et al., 2015; Zheng et al., 2016). Do they share any common properties? Could they be described by a unified model? We summed up several representative competition scenarios following the life cycle of gene expression (Figure 1), including competitions for transcription factors by DNA binding sites (Figure 1B), competitions for miRNAs and ribosomes by RNA molecules (Figure 1C and 1D), and competitions for degradation enzymes by target proteins (Figure 1E). Inspired by previous models studying ceRNA effect (Ala et al., 2013; Yuan et al., 2015), we proposed a generalized competition motif model, in which two target molecule species (target#1 and #2, T_1 and T_2) competitively bind with a shared regulatory molecule species (regulator, R) (Figure 1A), to describe the similar competition topology these cases share. In this model, each molecule species is produced and degraded with certain rates, and the regulator is dynamically bound to targets following biochemical mass-action laws to form complexes (Figure 1F, SI Material and Methods). Loss rates of regulator (α) and its competing targets (β) were introduced to describe reactions from pure stoichiometric ($\alpha \sim 1, \beta \sim 1$) to pure catalytic ($\alpha \sim 1, \beta \sim 0$ where enzymes act as competitors, or $\alpha \sim 0$, $\beta \sim 1$ when substrates act as competitors) (Ala et al., 2013). In different biochemical scenarios, experimentally measured signals may reflect different component levels of the competition motif. For example, the activity of targets could be mainly reflected by

the abundance of complexes (T^C) when the regulator is an activator, or by the abundance of the free targets (T^F) when the regulator is a repressor.

This unified model can describe competitions in various biological processes (Figure S1A-D). Despite of different parameter settings, all these cases share the core competition motif structure, suggesting that they may share common characteristics. In the following sections, we used this model to analyze, in the scenario of either steady-state behavior or dynamic response, how the competition introduces indirect regulations between targets and how the existence of the competitors influences the property of regulator-target response.

Relative abundance determines the regulatory patterns between competitors

Competition can cause crosstalk between targets. By quantifying the competition effect of one target upon the abundance of another target, recent studies have reported two apparently different steady-state behaviors named "threshold behavior" of ceRNA regulation in mammalian cells (Ala et al., 2013) and "negative linear dependence" behavior of synthetic gene expression in bacteria (Carbonell-Ballestero et al., 2016; Gyorgy et al., 2015). How could competition generate such two vastly different phenomena?

The model predicted that the relative abundance between regulator and target determines the diverse behaviors. Figure 2A and S2A illustrates how molecular abundance changes along with the gradual increment of T_2's production rate. The

system went through three regimes: "*R* abundant", "*R* near-equimolar" and "*R* scarce", which are mainly determined by the production rate and loss rate of each component (SI Material and Methods). In the "*R* abundant" regime, free T_1 level (T_1^F) is not sensitive to the increment of free T_2 level (T_2^F), but when the system enters the "*R* near-equimolar" regime, T_1^F becomes more sensitive to T_2^F changes, thus generates the threshold behavior (Figure 2B and S2B). In contrast, T_1 complex level (T_1^C) is substantially unchanged with respect to T_2 complex level (T_2^C) except in the "*R* scarce" regime, where T_1^C displays a negative linear dependence with T_2^C (Figure 2C).

In the case of ceRNA regulation, where miRNA is a repressor, target activity can be reflected by the free mRNA level. Increments of ceRNA$_2$ (T_2^F) can raise free ceRNA$_1$ (T_1^F) level indirectly by sequestering shared miRNAs. Such derepression caused by ceRNA effect is negligible when the level of ceRNA$_2$ is far less than that of miRNA (in the "*R* abundant" regime), but becomes detectable when the level of ceRNA$_2$ is comparable to that of miRNA (in the "*R* near-equimolar" regime) (Ala et al., 2013; Yuan et al., 2015). In contrast, when the regulator is an activator, target activity can be represented by the level of complexes. Recently a phenomenon called "isocost line" behavior, originally studied in economics, was also found in synthetic biological systems (Carbonell-Ballestero et al., 2016; Gyorgy et al., 2015) that the expressions of two fluorescent proteins in *E. coli* displayed negative linear dependence, which was caused by competition for the transcription and translation resources (acting as activator)

by the two synthetic genes. Due to the high expression level of these genes, the system was always restricted to the "*R* scarce" regime, thus showed negative linear dependence.

In summary, threshold behavior and negative linear dependence are two aspects generated by the same competition motif. The threshold behavior is observed when the regulator is a repressor and the system transfers from the "*R* abundant" to the "*R* near-equimolar" regime; while the negative linear dependence occurs when the regulator is an activator and the system is restricted to the "*R* scarce" regime.

Competition can shape dose-response curve

How does competition modulate the response of target to varying levels of a regulator? The dose-response curve, which quantitatively describes the magnitude of such responses, was systematically analyzed. Firstly, the dose-response curve of free T_1 (T_1^F) level to the total regulator (R) level without competition effect (without T_2) was calculated as the baseline. As expected (Buchler & Louis, 2008), T_1^F was not sensitive to the regulator changes in the "*R* scarce" regime, but became sensitive in the "*R* near-equimolar" regime, thus forming some "threshold behavior" (black line in Figure 2D-E). Then we analyzed how the molecular levels and the kinetic parameters of the competitor T_2 might influence the shape of the R-T_1^F dose-response curve. We first considered the case that T_1 and T_2 have the same kinetic parameters to bind R. Increments of T_2 production could elevate the maximum sensitivity to enhance the threshold behavior, and shift the position of the maximum sensitivity to a higher R level

in the new "*R* near-equimolar" regime (Figure 2D-E). We next fixed T_2's production rate and analyzed the influence of other kinetic parameters. The relative binding affinity was found as the key parameters to modulate the R-T_1^F dose-response curve. If T_2^C was formed slowly (small k_{2+}) or dissociated rapidly (large k_{2-}), T_2 could hardly alter the R-T_1^F response. Along with the increment of T_2 binding affinity (increasing k_{2+} or decreasing k_{2-}), T_2's competition blunted the sensitivity in the R~T_1 near-equimolar regime considering only R and T_1, meanwhile enhanced the sensitivity in the R~T_1+T_2 near-equimolar regime in the presence of T_2 (Figure 2F-G and S2C-E).

The model analysis is consistent with the experimental observations in diverse molecular competition scenarios reported previously. In the case of ceRNA (Figure 1C), the RNA competitors with comparable binding affinities can enhance the maximum sensitivity and shift their positions in the miRNA-target dose-response curve, and a higher competing RNA level can cause a stronger enhancement and shift (Yuan et al., 2015). Similarly, in the studies on the TF titration effect (Figure 1B), introducing high affinity competitive binding sites can greatly shift and sharpen the response of primary target gene expression to the TF (Brewster et al., 2014; Lee & Maheshri, 2012). In contrast, in the case of buffer solutions in chemistry, for example the ammonium buffer, the weak base NH_4^+ compete with H^+ for OH^-, and NH_4^+ has a much lower binding affinity with OH^- than H^+ (Figure S1E). When a mild change of OH^- (e.g. adding moderate amounts of NaOH or HCl) is introduced into the solution, NH_4^+ can buffer the response of free H^+ to OH^-, thus keeping pH (potential of hydrogen) almost constant

in a certain range (SI Material and Methods). In summary, introducing the competitors can shape the R-T_1^F dose-response curve. A high affinity competitor can enhance the maximum sensitivity and shift its position to a higher R level; while a low affinity competitor may buffer the response. The extents of such modulations are dictated by the abundance of competitors.

However, it should be noticed that when it comes to the response curve of a free primary target to the level of a free regulator (R^F-T_1^F), the curve was not influenced by the existence of competitor at all (Figure 2H). This is because, rather than the total regulator abundance, the free regulator abundance is the one effectively determines the kinetic reaction rate with each single target (Jens & Rajewsky, 2015). Thus, responses of two or more targets to the shared regulator are mutually independent given the level of R^F, which provides an efficient way, by using R^F level as the medium, to analyze the relative regulatory efficiency among multi-targets (Yuan et al., 2016). Once given the dose-response of each component (R^F-T_i^F, which could be separately measured or calculated) and the expected regulatory efficiency of a specific target, the level of all other targets could be immediately predicted because they are all exposed to the same free regulator level (Figure 2I, SI Material and Methods). Such property is especially important for designing synthetic circuits, where we know the characteristics of each single part and would like to predict the whole system's behavior when putting them together. This property has been applied to siRNA design principle: by both *in silico* simulation and experimental validation, we found that the influence of a high off-target

gene expression level could be compensated by introducing a suitable number of siRNAs, whereas off-target genes with strong binding affinity should be avoided (Yuan et al., 2015; Yuan et al., 2016). In summary, the dose-response to the free regulator level is not influenced by any competitors, therefore providing an efficient way to extract the relative response relations in multi-target networks.

Competition can delay or accelerate dynamic response

How does the existence of competitors influence the dynamic behavior of the system in response to a time-varying regulator? To answer this question, we simulated the response of a switching system with regulator level changing between "ON" and "OFF" states (Figure 3A). On the rising edge of R's change, the existence of T_2's competition always delays the response of both T_1^F and T_1^C, because it can sequester R from binding with T_1 and may cause additional R loss via T_2^C degradation, both of which resist the increment of available R to regulate T_1. However, on the falling edge, competing can either accelerate or delay the response depending on the kinetic parameters (Figure 3B-C and S3A-F, SI Material and Methods). On the one hand, T_2^C dissociation could compensate R's decrease, but on the other hand, T_2^C degradation may cause R loss, and these two opposing effects can dominate the final modulation of the dynamic response. T_2 with a large complex degradation rate (g_2) and a large loss rate (α_2) could lead to a quick response by mediating more R loss (Figure 3B); while T_2 with different binding affinities could either accelerate or delay the response under different parameter settings

(Figure 3C and S3C-F), because T_2 with a strong binding affinity can enhance both R compensation and R loss via T_2^C degradation at the same time.

Recently, it has been experimentally observed that the competition for LacI binding in *E. coli* delayed the rising edge response, but accelerated the falling edge response because of the loss of the regulator binding with targets through degradation and dilution (large α_2) (Jayanthi et al., 2013). On the contrary, the existence of competitive binding sites for transcription factor SKN7m in *S. cerevisiae* was found to delay the response of the primary target on both the rising and the falling edges (Mishra et al., 2014), which implied that the regulator might be protected from degradation when binding with targets (g_2 is small) (Burger et al., 2010; Jayanthi et al., 2013). In summary, competition can modulate the dynamic response of some targets to their upstream regulators. This may implicate a general parameter tuning method to adjust the response dynamics in the presence of the competitors.

Competition can modify target expression noise level

Competition can modulate the sensitivity and the speed of a target response to a changing regulator, both of which are highly relevant to target fluctuation (Blake et al., 2003; Chen et al., 2013). A natural question is how the existence of competitors may influence noise in the system? Here we took miRNA regulation as an example to analyze the noise level of protein products (Figure 3D, SI Material and Methods). In systems without R and T_2, T_1 expression noise is derived from fluctuations in

transcription, translation and degradation, and the coefficient of variance (CV) of T_1 gene expression approaches the "power law", as expected by the "$1/\sqrt{N}$ rule" proposed by Schrödinger (Schrödinger, 1944). The introduction of R (miRNA) as repressor can decrease the noise of lowly expressed genes, meanwhile generate a noise peak in the "R near-equimolar" regime for highly expressed genes (Figure 3E), consistent with previous studies (Bosia et al., 2017; Schmiedel et al., 2015).

Theoretical results indicated that the competition effect of T_2 could modify T_1 expression noise significantly. As expected, introducing T_2 weakens R's ability to suppress T_1, thus may impair the noise reduction in the low expression zone. Interestingly, in the high expression zone of T_1, T_2 with strong binding affinity with R may elevate T_1 noise level (Figure 3F); while T_2 with weak binding affinity may substantially depress T_1 noise level (Figure 3G). Therefore, comparing with the one-regulator-one-target scenario, introducing higher level of miRNAs and compensable weak competitors could reduce target expression noise at the low expression zone and suppress the noise peak introduced by miRNA at the high expression zone at the same time, thus could repress gene expression noise in a wide range (Figure 3H). In summary, competition effects may modulate gene expression noise level, and in particular, abundant weak competitors have the capability to buffer gene expression noise globally (Figure S3G-J).

Competition can introduce correlated fluctuation between targets

Competition can not only modify the strength of target fluctuation, but also couple fluctuations between these targets (Figure 3I). Dynamic analysis of the model's behavior around steady state with different molecular environments predicted that the free T_1 (T_1^F) and T_2 (T_2^F) are positively correlated (Figure 3J), while the competitor complexes (T_1^C and T_2^C) are negatively correlated (Figure 3K). The correlation strengths in both cases are maximized in the "*R* near-equimolar" regime, and gradually decrease with the system away from the regime.

This phenomenon has been predicted as the "correlation resonance" by some previous theoretical analysis on gene translation (Mather et al., 2013) and protein degradation (Cookson et al., 2011; Mather et al., 2010). Two kinds of proteins (T_1^F and T_2^F) competing for degradation enzyme ClpXP (*R*) showed positive correlated fluctuation, which reached the maximum when the sum of two protein production rates approached to the ClpXP's processing capacity (Cookson et al., 2011; Mather et al., 2010). Another theoretical analysis showed that in translation process, fluctuations of mRNA-ribosome complexes (T_1^C and T_2^C) were negatively correlated (Mather et al., 2013). In summary, competition can introduce negatively correlated fluctuation between free targets and positively correlated fluctuation between complexes, and both of their strength reach the maximum in the "*R* near-equimolar" regime.

Regulator allocation to multiple targets

Regulators often bind more than two target species simultaneously. How will regulator be allocated to multiple target species? A system with multiple targets competing for the same regulator can be described by the set of allocation equations (Figure 4A), where the proportion of the regulator occupied by a certain target in steady state is mainly determined by this target's abundance and its capabilities to bind to (and hence to consume) the regulator (SI Material and Methods). It was noticed that, the form of the regulator allocation equation is analogous to Kirchhoff's laws in current divider circuits, where R's production rate is analogous to the total current, the capability of T_i^C to consume R is analogous to the ith branch current, and the capability of T_i^F to occupy R is analogous to the ith branch conductance (the reciprocal of resistance) (Figure 4B). Therefore, electronic circuits and biological systems with competition may exhibit similar properties, such as the "negative linear dependence" behavior when resources are insufficient (in the "R scarce" regime) (Carbonell-Ballestero et al., 2016).

Such allocation equations have displayed in diverse mathematical models, such as the reaction rates of product formation in enzymatic reactions when multiple substrates competing for the same catalytic enzyme under the Michaelis-Menten kinetics (Chou & Talaly, 1977), and the probabilities of promoter-TF binding when multiple promoters competing for the same TF under the thermodynamic model (Bintu et al., 2005). Meanwhile, this property has helped quantify the allocations of the transcription or the translation resources for synthetic gene circuits (Carbonell-Ballestero et al., 2016; Qian et al., 2017). We also applied such property to predict the miRNA occupancy on each

target site in a specific cell type with the miRNA and the target RNA expression levels, and significantly improved the accuracy of the miRNA target prediction (Xie et al., 2014). Those miRNAs with significant occupancy changes during tumorigenesis could serve as potent biomarkers in addition to differentially expressed miRNAs.

Discussion

Competition for limited resources is ubiquitous throughout diverse molecular reactions in both natural and synthetic biological systems. Using a coarse-gained mathematical model, we systematically analyzed the steady-state behavior and the dynamic properties of various competition network motifs, from the view of indirect regulations among the competitors as well as the effects of the competitors on the regulator-target response (Table 1). It should be noticed that, most of the mentioned properties are connected with the concept of the *regimes* determined by the regulator-target relative abundance (Figure 2A-C): threshold behavior occurs when system transfers from the "*R* abundant" to the "*R* near-equimolar" regime, and linear negative dependence happens when system is in the "*R* scarce" regime; while the sensitivity of the dose-response curve, the correlated fluctuation, and the noise of the target level are all maximized in the "*R* near-equimolar" regime.

Competition motif is a common network component. It seldom functions as an isolated module in real-world biological systems, but often interacts with other components to form complex networks. For example, simulation analysis on ceRNA

regulation suggested that additional targets and regulators connected with different topology could enhance or weaken the ceRNA effect (Ala et al., 2013). Theoretical analysis predicted that competition for degradation enzyme could either promote or suppress the robustness of biological oscillating circuit with different topological structures (Rondelez, 2012). In addition, competition motif could perform a variety of functions by combining with other network motifs. For example, cooperating with the positive feedback motif, competition can generate the winner-take-all (WTA) behavior (Kim et al., 2004), which have been applied to design *in vitro* molecular circuits for supervised learning and pattern classification using DNA strand displacement (Genot et al., 2013; Lakin & Stefanovic, 2016).

The unified competition model gives inspirations for transferring knowledge among different molecular scenarios, since similar molecular network topology may perform similar functions. For example, the case that ceRNA competition can sharpen the dose-response curve of miRNA regulation (Yuan et al., 2015) is quite similar to that observed for TF titration effect (Brewster et al., 2014). Such generality and feasibility give us confidence to make new predictions based on the competition model. For instance, the properties of pH buffer solutions demonstrated that some weak competitors could desensitize the response of the primary target to the regulator, which implies the potential role of many competitors as noise buffer. Functions of numerous miRNA target sites have long been a mystery that each miRNA species in mammalian cell could bind to hundreds target RNA species, but only a small portion of the targets

368 with multiple high affinity binding sites could be moderately repressed (rarely exceeds
369 2-folds). That is to say, in most cases, miRNA binding are not functioned as intensive
370 repression (Seitz, 2009). Why are there so many evolutionary conserved miRNAs and
371 potential targets if this is an inefficient regulatory mechanism? The competition model
372 provides a possible explanation that such widespread miRNA competitors with low
373 binding affinity could buffer noise and stabilize gene expression.

374 Competition effect is one of the major challenges for circuits design in synthetic
375 biology. Synthetic gene expression can lead to intracellular resource reallocation, which
376 may affect the performance of both exogenous gene circuits and host gene networks
377 simultaneously. It may change the network structure of the original designed circuits
378 by introducing a hidden layer of regulation, making it difficult to predict the whole
379 circuit's behavior based on the characteristic of each individual component. For
380 example, competition for cellular resources may reshape the response of genetic
381 activation cascades in *E. coli* (Qian et al., 2017), and multiple downstream genes
382 competing for upstream signal molecules may accentuate the "retroactivity" (Brophy
383 & Voigt, 2014). It has been found that the induction strength of the synthetic gene
384 oscillator could influence the growth rate of host cell, the expression of endogenous
385 genes, and the performance of the oscillator, such as amplification and period (Weisse
386 et al., 2015). On the other hand, interestingly, using competition effect properly to
387 rebalance synthetic circuits' relation to the host cell is emerging as an effective way to
388 refine circuits performance. For example, the robustness of the synthetic oscillator can

389 be greatly improved by introducing competing binding sites for TF LacI to sharpen
390 target gene dose response curves and suppress gene expression noise (Potvin-Trottier
391 et al., 2016). Models incorporating circuit-host competition effects can predict synthetic
392 gene behaviors better (Liao et al., 2017). Reallocating the cellular translational
393 resources by introducing the endoribonuclease MazF circuit can significantly enhance
394 exogenous enzyme expression to promote metabolite production (Venturelli et al.,
395 2017). Utilizing synthetic miRNA and its competitive binding RNA sponges, a RNA-
396 based AND gate circuit was designed for selectively triggering T cell-mediated killing
397 of cancer cells (Nissim et al., 2017).

398 As discussed in this paper, competition of molecules matters in diverse biological
399 processes, not only convoluting regulations in cell, but also introducing plentiful
400 functions. The concept of competition motifs and its coarse-gained model may provide
401 a unified insight to understand diverse molecular competition phenomena, and
402 modulate biological networks by coupling or decoupling components on the hidden
403 layer.

404

405 **Materials and Methods**

406 Detailed information about mathematical derivations and simulations is available in SI
407 Materials and Methods. Parameters for simulations are shown in Table S1.

408

409 **Acknowledgements**

This work has been supported by the National Science Foundation of China Grants (No. 61773230, 31371341, 61721003, 91730301, 31671384, 91729301), National Basic Research Program of China (2017YFA0505503), Initiative Scientific Research Program (No. 20141081175) and Cross-discipline Foundation of Tsinghua University, and the Open Research Fund of State Key Laboratory of Bioelectronics Southeast University.

Conflict of Interests

The authors declare that they have no conflict of interest.

References

Ala, U., Karreth, F. A., Bosia, C., Pagnani, A., Taulli, R., Leopold, V., Tay, Y., Provero, P., Zecchina, R., & Pandolfi, P. P. (2013). Integrated transcriptional and competitive endogenous RNA networks are cross-regulated in permissive molecular environments. *Proc Natl Acad Sci U S A, 110*(18), 7154-7159. doi:10.1073/pnas.1222509110

Bintu, L., Buchler, N. E., Garcia, H. G., Gerland, U., Hwa, T., Kondev, J., & Phillips, R. (2005). Transcriptional regulation by the numbers: models. *Curr Opin Genet Dev, 15*(2), 116-124. doi:10.1016/j.gde.2005.02.007

Blake, W. J., M, K. A., Cantor, C. R., & Collins, J. J. (2003). Noise in eukaryotic gene expression. *Nature, 422*(6932), 633-637. doi:10.1038/nature01546

Bolnick, D. I. (2004). Can Intraspecific Competition Drive Disruptive Selection? An Experimental Test in Natural Populations of Sticklebacks. *Evolution, 58*(3). doi:10.1554/03-326

Bosia, C., Sgro, F., Conti, L., Baldassi, C., Brusa, D., Cavallo, F., Cunto, F. D., Turco, E., Pagnani, A., & Zecchina, R. (2017). RNAs competing for microRNAs mutually influence their fluctuations in a highly non-linear microRNA-dependent manner in single cells. *Genome Biol, 18*(1), 37. doi:10.1186/s13059-017-1162-x

Brewster, R. C., Weinert, F. M., Garcia, H. G., Song, D., Rydenfelt, M., & Phillips, R. (2014). The transcription factor titration effect dictates level of gene expression. *Cell, 156*(6), 1312-1323. doi:10.1016/j.cell.2014.02.022

Brophy, J. A., & Voigt, C. A. (2014). Principles of genetic circuit design. *Nat Methods, 11*(5), 508-520. doi:10.1038/nmeth.2926

Buchler, N. E., & Louis, M. (2008). Molecular titration and ultrasensitivity in regulatory networks. *J Mol Biol, 384*(5), 1106-1119. doi:10.1016/j.jmb.2008.09.079

Burger, A., Walczak, A. M., & Wolynes, P. G. (2010). Abduction and asylum in the lives of transcription factors. *Proc Natl Acad Sci U S A, 107*(9), 4016-4021. doi:10.1073/pnas.0915138107

Carbonell-Ballestero, M., Garcia-Ramallo, E., Montanez, R., Rodriguez-Caso, C., & Macia, J. (2016). Dealing with the genetic load in bacterial synthetic biology circuits: convergences with the Ohm's law. *Nucleic Acids Res, 44*(1), 496-507. doi:10.1093/nar/gkv1280

448 Cardinale, S., & Arkin, A. P. (2012). Contextualizing context for synthetic biology--identifying causes
449 of failure of synthetic biological systems. *Biotechnol J, 7*(7), 856-866.
450 doi:10.1002/biot.201200085
451 Cesana, M., Cacchiarelli, D., Legnini, I., Santini, T., Sthandier, O., Chinappi, M., Tramontano, A., &
452 Bozzoni, I. (2011). A long noncoding RNA controls muscle differentiation by functioning as a
453 competing endogenous RNA. *Cell, 147*(2), 358-369. doi:10.1016/j.cell.2011.09.028
454 Chang, C. H., Qiu, J., O'Sullivan, D., Buck, M. D., Noguchi, T., Curtis, J. D., Chen, Q., Gindin, M.,
455 Gubin, M. M., van der Windt, G. J., Tonc, E., Schreiber, R. D., Pearce, E. J., & Pearce, E. L.
456 (2015). Metabolic Competition in the Tumor Microenvironment Is a Driver of Cancer
457 Progression. *Cell, 162*(6), 1229-1241. doi:10.1016/j.cell.2015.08.016
458 Chen, M., Wang, L., Liu, C. C., & Nie, Q. (2013). Noise attenuation in the ON and OFF states of
459 biological switches. *ACS Synth Biol, 2*(10), 587-593. doi:10.1021/sb400044g
460 Chou, T.-C., & Talaly, P. (1977). A simple generalized equation for the analysis of multiple inhibitions
461 of Michaelis-Menten kinetic systems. *Journal of Biological Chemistry, 252*(18), 6438-6442.
462 Connell, J. H. (1983). On the Prevalence and Relative Importance of Interspecific Competition:
463 Evidence from Field Experiments. *The American Naturalist, 122*(5), 661-696.
464 doi:10.1086/284165
465 Cookson, N. A., Mather, W. H., Danino, T., Mondragon-Palomino, O., Williams, R. J., Tsimring, L. S.,
466 & Hasty, J. (2011). Queueing up for enzymatic processing: correlated signaling through
467 coupled degradation. *Mol Syst Biol, 7*, 561. doi:10.1038/msb.2011.94
468 Genot, A. J., Fujii, T., & Rondelez, Y. (2013). Scaling down DNA circuits with competitive neural
469 networks. *J R Soc Interface, 10*(85), 20130212. doi:10.1098/rsif.2013.0212
470 Gorochowski, T. E., Avcilar-Kucukgoze, I., Bovenberg, R. A., Roubos, J. A., & Ignatova, Z. (2016). A
471 Minimal Model of Ribosome Allocation Dynamics Captures Trade-offs in Expression between
472 Endogenous and Synthetic Genes. *ACS Synth Biol, 5*(7), 710-720.
473 doi:10.1021/acssynbio.6b00040
474 Gyorgy, A., Jimenez, J. I., Yazbek, J., Huang, H. H., Chung, H., Weiss, R., & Del Vecchio, D. (2015).
475 Isocost Lines Describe the Cellular Economy of Genetic Circuits. *Biophys J, 109*(3), 639-646.
476 doi:10.1016/j.bpj.2015.06.034
477 Hardin, G. (1960). The Competitive Exclusion Principle. *Science, 131*(3409), 1292-1297.
478 doi:10.1126/science.131.3409.1292
479 Hui, S., Silverman, J. M., Chen, S. S., Erickson, D. W., Basan, M., Wang, J., Hwa, T., & Williamson, J.
480 R. (2015). Quantitative proteomic analysis reveals a simple strategy of global resource
481 allocation in bacteria. *Mol Syst Biol, 11*(1), 784. doi:10.15252/msb.20145697
482 Jayanthi, S., Nilgiriwala, K. S., & Del Vecchio, D. (2013). Retroactivity controls the temporal
483 dynamics of gene transcription. *ACS Synth Biol, 2*(8), 431-441. doi:10.1021/sb300098w
484 Jens, M., & Rajewsky, N. (2015). Competition between target sites of regulators shapes post-
485 transcriptional gene regulation. *Nat Rev Genet, 16*(2), 113-126. doi:10.1038/nrg3853
486 Jiang, P., Ventura, A. C., Sontag, E. D., Merajver, S. D., Ninfa, A. J., & Del Vecchio, D. (2011). Load-
487 induced modulation of signal transduction networks. *Sci Signal, 4*(194), ra67.
488 doi:10.1126/scisignal.2002152

Johnston, L. A. (2009). Competitive interactions between cells: death, growth, and geography. *Science, 324*(5935), 1679-1682. doi:10.1126/science.1163862

Khare, A., & Shaulsky, G. (2006). First among equals: competition between genetically identical cells. *Nat Rev Genet, 7*(7), 577-583. doi:10.1038/nrg1875

Kim, J., Hopfield, J., & Winfree, E. (2004). *Neural Network Computation by In Vitro Transcriptional Circuits.* Paper presented at the Advances in Neural Information Processing Systems.

Laird, A. K. (1964). Dynamics of Tumor Growth. *British Journal of Cancer, 18*(3), 490-502. doi:10.1038/bjc.1964.55

Lakin, M. R., & Stefanovic, D. (2016). Supervised Learning in Adaptive DNA Strand Displacement Networks. *ACS Synth Biol, 5*(8), 885-897. doi:10.1021/acssynbio.6b00009

Lee, T. H., & Maheshri, N. (2012). A regulatory role for repeated decoy transcription factor binding sites in target gene expression. *Mol Syst Biol, 8*, 576. doi:10.1038/msb.2012.7

Liao, C., Blanchard, A. E., & Lu, T. (2017). An integrative circuit-host modelling framework for predicting synthetic gene network behaviours. *Nat Microbiol, 2*(12), 1658-1666. doi:10.1038/s41564-017-0022-5

Mather, W. H., Cookson, N. A., Hasty, J., Tsimring, L. S., & Williams, R. J. (2010). Correlation resonance generated by coupled enzymatic processing. *Biophys J, 99*(10), 3172-3181. doi:10.1016/j.bpj.2010.09.057

Mather, W. H., Hasty, J., Tsimring, L. S., & Williams, R. J. (2013). Translational cross talk in gene networks. *Biophys J, 104*(11), 2564-2572. doi:10.1016/j.bpj.2013.04.049

Mishra, D., Rivera, P. M., Lin, A., Del Vecchio, D., & Weiss, R. (2014). A load driver device for engineering modularity in biological networks. *Nat Biotechnol, 32*(12), 1268-1275. doi:10.1038/nbt.3044

Nissim, L., Wu, M. R., Pery, E., Binder-Nissim, A., Suzuki, H. I., Stupp, D., Wehrspaun, C., Tabach, Y., Sharp, P. A., & Lu, T. K. (2017). Synthetic RNA-Based Immunomodulatory Gene Circuits for Cancer Immunotherapy. *Cell, 171*(5), 1138-1150 e1115. doi:10.1016/j.cell.2017.09.049

Potvin-Trottier, L., Lord, N. D., Vinnicombe, G., & Paulsson, J. (2016). Synchronous long-term oscillations in a synthetic gene circuit. *Nature, 538*(7626), 514-517. doi:10.1038/nature19841

Qian, Y., Huang, H. H., Jimenez, J. I., & Del Vecchio, D. (2017). Resource Competition Shapes the Response of Genetic Circuits. *ACS Synth Biol, 6*(7), 1263-1272. doi:10.1021/acssynbio.6b00361

Rondelez, Y. (2012). Competition for catalytic resources alters biological network dynamics. *Phys Rev Lett, 108*(1), 018102. doi:10.1103/PhysRevLett.108.018102

Saha, S., Weber, C. A., Nousch, M., Adame-Arana, O., Hoege, C., Hein, M. Y., Osborne-Nishimura, E., Mahamid, J., Jahnel, M., Jawerth, L., Pozniakovski, A., Eckmann, C. R., Julicher, F., & Hyman, A. A. (2016). Polar Positioning of Phase-Separated Liquid Compartments in Cells Regulated by an mRNA Competition Mechanism. *Cell, 166*(6), 1572-1584 e1516. doi:10.1016/j.cell.2016.08.006

Schmiedel, J. M., Klemm, S. L., Zheng, Y., Sahay, A., Bluthgen, N., Marks, D. S., & van Oudenaarden, A. (2015). Gene expression. MicroRNA control of protein expression noise. *Science, 348*(6230), 128-132. doi:10.1126/science.aaa1738

Schoener, T. W. (1983). Field Experiments on Interspecific Competition. *The American Naturalist, 122*(2), 240-285. doi:10.1086/284133

Schrödinger, E. (1944). *What is life?* : Cambridge University Press.

Scott, M., Gunderson, C. W., Mateescu, E. M., Zhang, Z., & Hwa, T. (2010). Interdependence of cell growth and gene expression: origins and consequences. *Science, 330*(6007), 1099-1102. doi:10.1126/science.1192588

Seitz, H. (2009). Redefining microRNA targets. *Curr Biol, 19*(10), 870-873. doi:10.1016/j.cub.2009.03.059

Sigova, A. A., Abraham, B. J., Ji, X., Molinie, B., Hannett, N. M., Guo, Y. E., Jangi, M., Giallourakis, C. C., Sharp, P. A., & Young, R. A. (2015). Transcription factor trapping by RNA in gene regulatory elements. *Science, 350*(6263), 978-981. doi:10.1126/science.aad3346

Sumazin, P., Yang, X., Chiu, H. S., Chung, W. J., Iyer, A., Llobet-Navas, D., Rajbhandari, P., Bansal, M., Guarnieri, P., Silva, J., & Califano, A. (2011). An extensive microRNA-mediated network of RNA-RNA interactions regulates established oncogenic pathways in glioblastoma. *Cell, 147*(2), 370-381. doi:10.1016/j.cell.2011.09.041

Svanback, R., & Bolnick, D. I. (2007). Intraspecific competition drives increased resource use diversity within a natural population. *Proc Biol Sci, 274*(1611), 839-844. doi:10.1098/rspb.2006.0198

Venturelli, O. S., Tei, M., Bauer, S., Chan, L. J. G., Petzold, C. J., & Arkin, A. P. (2017). Programming mRNA decay to modulate synthetic circuit resource allocation. *Nat Commun, 8*, 15128. doi:10.1038/ncomms15128

Weisse, A. Y., Oyarzun, D. A., Danos, V., & Swain, P. S. (2015). Mechanistic links between cellular trade-offs, gene expression, and growth. *Proc Natl Acad Sci U S A, 112*(9), E1038-1047. doi:10.1073/pnas.1416533112

Wu, G., Yan, Q., Jones, J. A., Tang, Y. J., Fong, S. S., & Koffas, M. A. G. (2016). Metabolic Burden: Cornerstones in Synthetic Biology and Metabolic Engineering Applications. *Trends Biotechnol, 34*(8), 652-664. doi:10.1016/j.tibtech.2016.02.010

Xie, P., Liu, Y., Li, Y., Zhang, M. Q., & Wang, X. (2014). MIROR: a method for cell-type specific microRNA occupancy rate prediction. *Mol Biosyst, 10*(6), 1377-1384. doi:10.1039/c3mb70610a

Yuan, Y., Liu, B., Xie, P., Zhang, M. Q., Li, Y., Xie, Z., & Wang, X. (2015). Model-guided quantitative analysis of microRNA-mediated regulation on competing endogenous RNAs using a synthetic gene circuit. *Proc Natl Acad Sci U S A, 112*(10), 3158-3163. doi:10.1073/pnas.1413896112

Yuan, Y., Ren, X., Xie, Z., & Wang, X. (2016). A quantitative understanding of microRNA-mediated competing endogenous RNA regulation. *Quantitative Biology, 4*(1), 47-57. doi:10.1007/s40484-016-0062-5

Zheng, Q., Bao, C., Guo, W., Li, S., Chen, J., Chen, B., Luo, Y., Lyu, D., Li, Y., Shi, G., Liang, L., Gu, J., He, X., & Huang, S. (2016). Circular RNA profiling reveals an abundant circHIPK3 that regulates cell growth by sponging multiple miRNAs. *Nat Commun, 7*, 11215. doi:10.1038/ncomms11215

Zwietering, M., Jongenburger, I., Rombouts, F., & Van't Riet, K. (1990). Modeling of the bacterial growth curve. *Applied and environmental microbiology, 56*(6), 1875-1881.

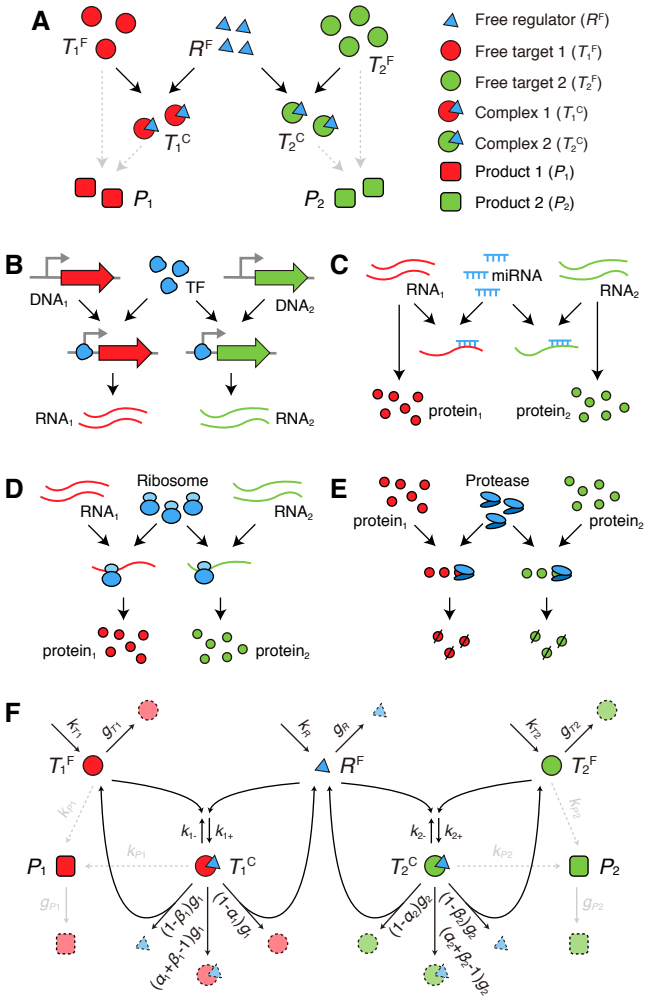

Figure 1 The coarse-gained competition motif model.

(A) Basic structure of the competition motif. Downstream products can be produced from either free targets or complexes.

(B-E) Competition motifs abstracted from diverse competition scenarios: (B) DNA binding sites competing for TFs; (C) RNA molecules competing for miRNAs; (D) mRNA molecules competing for ribosomes; (E) proteins competing for proteases.

(F) Unified kinetic model of the competition motif.

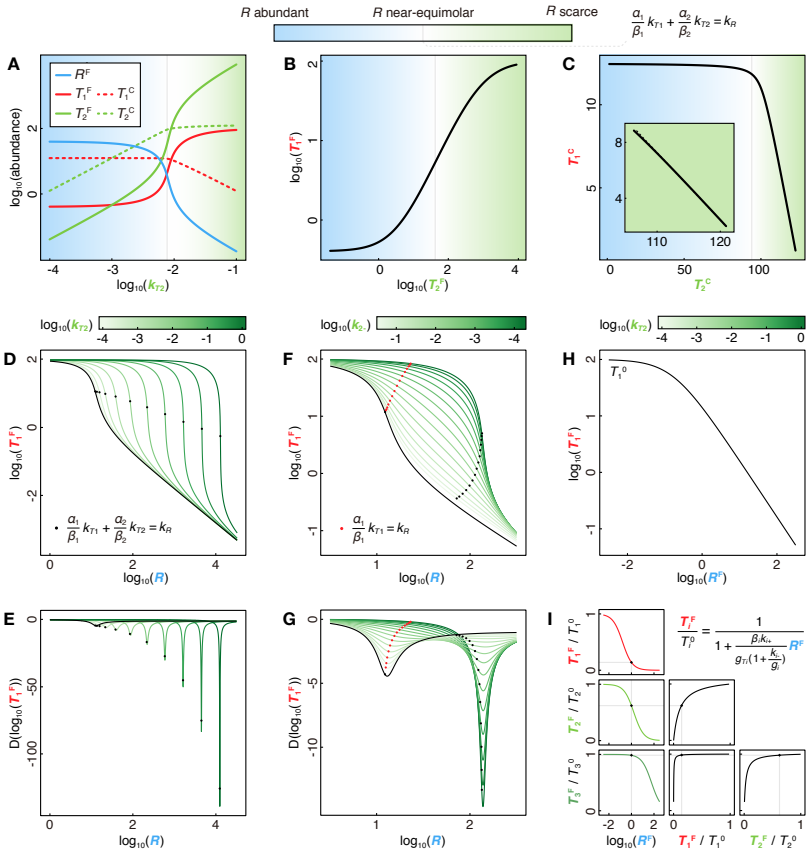

Figure 2 Steady state behaviors of competition systems.

(A-C) Regimes of competition systems. (A) Abundances changes of each component with the increment of T_2's production rate (k_{T2}). (B) Abundance of T_1^F as a function of that of T_2^F. (C) Abundance of T_1^C as a function of that of T_2^C. Blue, white and green areas represent "*R* abundant", "*R* near-equimolar" and "*R* scarce" regime respectively. Grey lines represent the approximate threshold (SI Materials and Methods).

(D-G) Dose-response curves modulated by competition. (D-E) *R*-T_1^F dose-response curves (D) and their derivatives (E) with different T_2's production rate (k_{T2}). (F-G) *R*-T_1^F dose-response curves (F) and their derivatives (G) with different T_2^C's dissociation rate ($k_{2\text{-}}$). *R* represents the total abundance of regulator ($R^F+T_1^C+T_2^C$). Black lines represent the dose response curve without T_2 (k_{T2}=0).

(H) R^F-T_1 dose-response curves with different k_{T2}. T_1^0 represents the abundance of T_1^F without *R*. Black line represents the dose response curve without T_2 (k_{T2}=0). All the curves with different k_{T2} are exactly overlapped.

(I) Repression folds of all targets are determined by the same R^F abundance in a multi-target repression system.

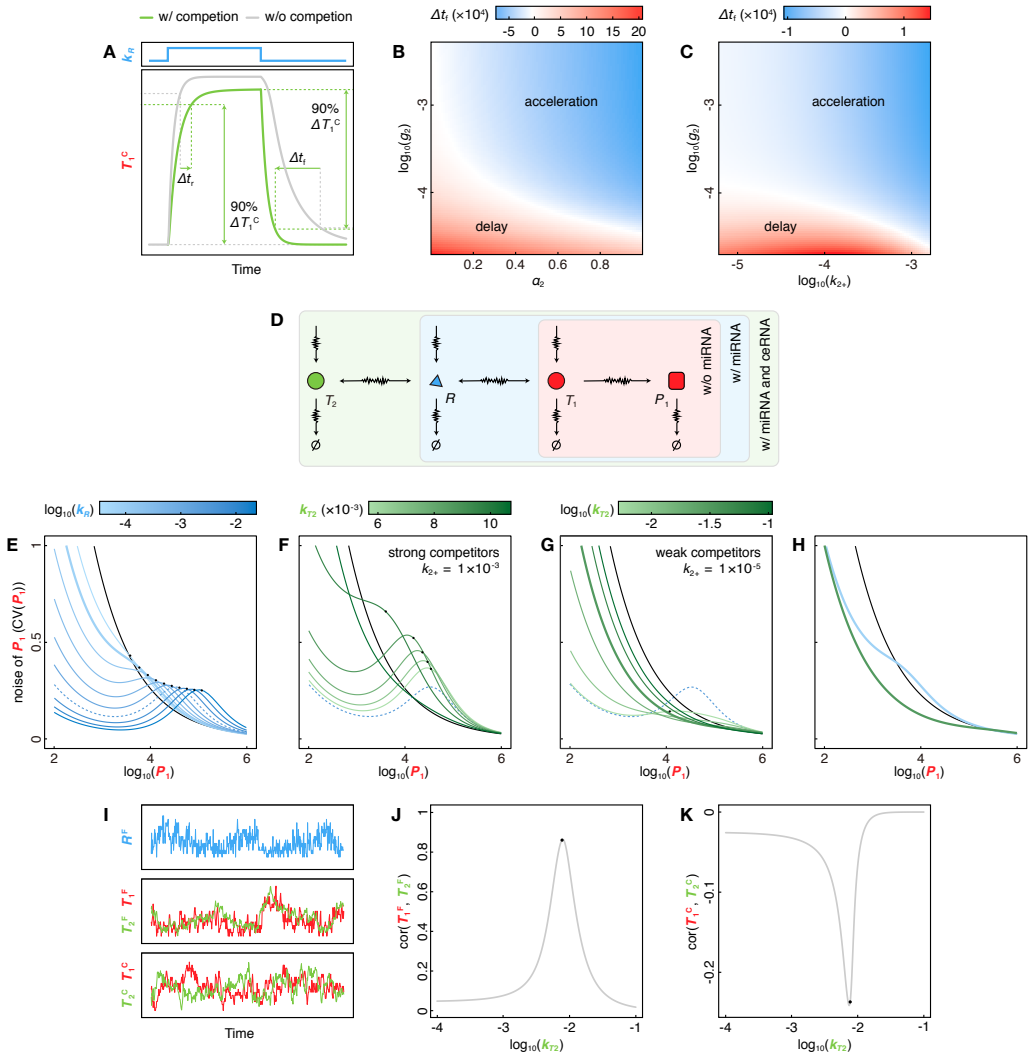

Figure 3 Dynamic properties of competition systems.

(A) Quantitative measurements of response time. Δt_r and Δt_f represent the alteration of response time on the rising and falling edge of R's change respectively. Here response time is defined as the time taken by $T_1{}^C$ level to change from 0% to 90% between its initial and final steady states.

(B-C) Heatmaps of Δt_f under different α_2 and g_2 (B), or k_{2+} and g_2 (C).

(D) Schematic diagram of the target expression noise in the miRNA-target competition scenario.

(E-H) Modification of target expression noise by competition. (E) Product expression noise (CV(P_1)) with different R's production rates (k_R). (F) CV(P_1) with different T_2's production rates (k_{T2}) where T_2 acts as a strong competitor. (G) CV(P_1) with different k_{T2} where T_2 acts as a weak competitor. (H) Comparison of CV(P_1) with or without

competition. Here miRNA-RNA competing system is taken as an example. Black lines represent system without R. Dashed blue lines are highlighted as the basal lines in (F) and (G). The thick blue and green lines in (H) are taken from (E) and (G) respectively. Black dots represent the approximate threshold (there are no black dots on some curves because k_{T2} is too large to form the threshold).

(I-K) Correlated fluctuations introduced by competition. (I) Stochastic simulations of each component's abundance in competition motif. (J-K) Correlations of T_1^F and T_2^F (J), or T_1^C and T_2^C (K) changing with T_2's production rate (k_{T2}). Black dots represent the approximate threshold.

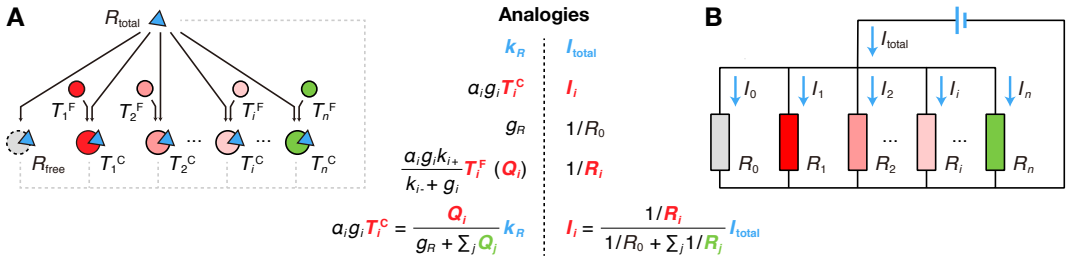

Figure 4 Regulator allocation for multi-target competition.

(A) Regulator allocation equations and schematic graph representation. R_{total} represent the total abundance of regulator, including free regulator and regulator in complexes.

(B) Kirchhoff's laws in current divider circuits.

Table 1 Properties of regulation by competition

	Regulation between targets	**Influences on regulator-target response**
Steady-state behavior	Threshold behavior Negative linear dependence Regulator allocation	Shaping dose-response curves
Dynamic responses	Correlated fluctuation	Response time modulation Noise modification

SI Materials and Methods

1. A unified coarse-gained competition motif model.

Parameters involved in the competition motif model (Figure 1F) where two target molecule species (target#1 and #2, T_1 and T_2) competitively bind with a shared regulatory molecule species (regulator, R) are described as follows. In general, T_1, T_2 or R is produced with a rate of k_{T1}, k_{T2} or k_R, respectively. Free T_1 (T_1^{F}), T_2 (T_2^{F}) or R (R^{F}) degrades at a rate of g_{T1}, g_{T2} or g_R. T_1^{F} or T_2^{F} binds to R^{F} to form target-regulator complex T_1^{C} or T_2^{C} at a rate of k_{1+} or k_{2+}, and T_1^{C} or T_2^{C} dissociates into R^{F} and T_1^{F} or T_2^{F} at a rate of k_{1-} or k_{2-}. T_1^{C} or T_2^{C} degrades at a rate of g_1 or g_2. Regulators on the complex degrade with the possibility of α_1 or α_2, and targets on the complex degrade with the possibility of β_1 or β_2, thus regulator would recycle from T_1^{C} or T_2^{C} with the possibility of $1-\alpha_1$ or $1-\alpha_2$, target would recycle from T_1^{C} or T_2^{C} with the possibility of $1-\beta_1$ or $1-\beta_2$, and regulator and target would degrade together with the possibility of $\alpha_1+\beta_1-1$ or $\alpha_2+\beta_2-1$. When R is a repressor, T_1^{F} or T_2^{F} may generate production P_1 or P_2 at a rate of k_{P1} or k_{P2}. In contrast, when R is an activator, T_1^{C} or T_2^{C} may generate production P_1 or P_2 at a rate of k_{P1} or k_{P2}. P_1 or P_2 degrades at a rate of g_{P1} or g_{P2}.

The competing model is described in the following differential equations:

$$\frac{\mathrm{d}\,R^{\mathrm{F}}}{\mathrm{d}\,t} = k_R - g_R R^{\mathrm{F}} - (k_{1+}T_1^{\mathrm{F}} + k_{2+}T_2^{\mathrm{F}})R^{\mathrm{F}} + k_{1-}T_1^{\mathrm{C}} + k_{2-}T_2^{\mathrm{C}} + (1-\alpha_1)g_1T_1^{\mathrm{C}} + (1-\alpha_2)g_2T_2^{\mathrm{C}} \quad [1]$$

$$\frac{\mathrm{d}\,T_1^{\mathrm{F}}}{\mathrm{d}\,t} = k_{T1} - g_{T1}T_1^{\mathrm{F}} - k_{1+}T_1^{\mathrm{F}}R^{\mathrm{F}} + k_{1-}T_1^{\mathrm{C}} + (1-\beta_1)g_1T_1^{\mathrm{C}} \quad [2]$$

$$\frac{\mathrm{d}\,T_1^{\mathrm{C}}}{\mathrm{d}\,t} = k_{1+}T_1^{\mathrm{F}}R^{\mathrm{F}} - k_{1-}T_1^{\mathrm{C}} - g_1T_1^{\mathrm{C}} \quad [3]$$

$$\frac{\mathrm{d}\,T_2^{\mathrm{F}}}{\mathrm{d}\,t} = k_{T2} - g_{T2}T_2^{\mathrm{F}} - k_{2+}T_2^{\mathrm{F}}R^{\mathrm{F}} + k_{2-}T_2^{\mathrm{C}} + (1-\beta_2)g_2T_2^{\mathrm{C}} \quad [4]$$

$$\frac{\mathrm{d}\,T_2^{\mathrm{C}}}{\mathrm{d}\,t} = k_{2+}T_2^{\mathrm{F}}R^{\mathrm{F}} - k_{2-}T_2^{\mathrm{C}} - g_2T_2^{\mathrm{C}} \quad [5]$$

We used this model to describe competitions in various biological processes. In the competition for TF by DNA binding sites (Figure 1B), T_1 and T_2 represent TF binding sites on DNA and R represents TF. The production and degradation rates of DNA binding sites are set to zero because they are negligible. Complexes degrade with only TF loss ($\alpha \sim 1$, $\beta \sim 0$). When g_1 or g_2 are set to zero, there is no TF loss. For TF as activator, DNA-TF complexes (T_1^{C} and T_2^{C}) can be transcribed into RNA, while for TF as repressor, free DNAs (T_1^{F} and T_2^{F}) can be transcribed (Figure S1A). In the competition for miRNA by RNA molecules (Figure 1C), T_1 and T_2 represent

two RNA molecule species and R represents miRNA. The loss of miRNA is relatively small so β is set to zero (Figure S1B) and as miRNA acts as a repressor, only free RNAs (T_1^{F} and T_2^{F}) translate into proteins. In the case of ribosome allocation (Figure 1D), where T_1 and T_2 represent two RNA molecule species and R represents ribosome, β is also set to zero (Figure S1C). In protein degradation competition (Figure 1E), where T_1 and T_2 represent two protein molecule species and R represents the protein degradation machine, β is set to zero too (Figure S1D). The topology of miRNA-target competition, ribosome-mRNA competition and protein degradation competition are identical except that components generating further production are different.

2. Theoretically analysis for molecular environment determining shapes of the regulation between competitors.

2.1. Solving steady states. Eqs. 1-5 can be solved for steady state when giving all differentials as zero. By adding Eqs. 2 and 3 , we get

$$T_1^{\mathrm{C}} = \frac{k_{T1} - T_1^{\mathrm{F}} g_{T1}}{\beta_1 g_1} \quad [6]$$

By adding Eqs. 1, 3 and 5, we get

$$R^{\mathrm{F}} = \frac{k_R - \alpha_1 T_1^{\mathrm{C}} g_1 - \alpha_2 T_2^{\mathrm{C}} g_2}{g_R} \quad [7]$$

Combining Eqs. 6 and 7, we get

$$R^{\mathrm{F}} = \frac{k_R - \frac{\alpha_1}{\beta_1}(k_{T1} - T_1^{\mathrm{F}} g_{T1}) - \frac{\alpha_2}{\beta_2}(k_{T2} - T_2^{\mathrm{F}} g_{T2})}{g_R} \quad [8]$$

Substituting Eqs. 6 and 8 into Eq. 3, we get

$$(T_1^{\mathrm{F}})^2 - T_1^{\mathrm{F}}(T_1^0 - \lambda_1 - \theta_1 + \phi_{21}) - \lambda_1 T_1^0 = 0 \quad [9]$$

Where

$$T_1^0 = \frac{k_{T1}}{g_{T1}} \qquad T_2^0 = \frac{k_{T2}}{g_{T2}} \quad [10]$$

$$\lambda_1 = \frac{g_R}{\alpha_1 k_{1+}}\left(\frac{k_{1-}}{g_1} + 1\right) \qquad \lambda_2 = \frac{g_R}{\alpha_2 k_{2+}}\left(\frac{k_{2-}}{g_2} + 1\right) \quad [11]$$

$$\gamma_1 = \frac{\beta_1}{\alpha_1 g_{T1}} \qquad \gamma_2 = \frac{\beta_2}{\alpha_2 g_{T2}} \quad [12]$$

$$\theta_1 = \gamma_1 k_R \qquad \theta_2 = \gamma_2 k_R \quad [13]$$

$$\phi_{21} = \frac{\gamma_1}{\gamma_2}(T_2^0 - T_2^{\mathrm{F}}) \qquad \phi_{12} = \frac{\gamma_2}{\gamma_1}(T_1^0 - T_1^{\mathrm{F}}) \quad [14]$$

Parameters were lumped to represent certain physical meanings to simplify the result. T_i^0 represents the free level of target $\#i$ (T_i) without regulators. $1/\lambda_i$ is proportional to k_{i+}, and negatively correlated with k_{i-}, thus could reflect the strength of binding affinity between T_i and regulator. θ is proportional to k_R, thus could reflect the level of regulator. ϕ_{ji} exhibits the competing regulation effects by target $\#j$ upon to target $\#i$.

Eq. 9 is a quadratic equation of T_1^{F}. Thus, the steady state abundance of free targets can be expressed as

$$T_1^{\mathrm{F}} = \frac{1}{2}(T_1^0 - \lambda_1 - \theta_1 + \phi_{21} + \sqrt{(T_1^0 - \lambda_1 - \theta_1 + \phi_{21})^2 + 4\lambda_1 T_1^0}) \quad [15]$$

$$T_2^{\mathrm{F}} = \frac{1}{2}(T_2^0 - \lambda_2 - \theta_2 + \phi_{12} + \sqrt{(T_2^0 - \lambda_2 - \theta_2 + \phi_{12})^2 + 4\lambda_2 T_2^0}) \quad [16]$$

2.2. Explanations on regimes and related phenomena. Assuming that the binding between targets and regulator is very strong, λ_i becomes negligible, thus Eq. 15 can be simplified as follows:

$$T_1^{\mathrm{F}} \simeq \begin{cases} \dfrac{\lambda_1 T_1^0}{\theta_1 - T_1^0 - \frac{\gamma_1}{\gamma_2}(T_2^0 - T_2^{\mathrm{F}})} \simeq 0 & , \text{if } T_1^0 + \phi_{21} < \theta_1 \\ T_1^0 - \theta_1 + \dfrac{\gamma_1}{\gamma_2}(T_2^0 - T_2^{\mathrm{F}}) & , \text{if } T_1^0 + \phi_{21} > \theta_1 \end{cases} \quad [17]$$

Meanwhile, the steady-state abundance of T_1^{C} and T_2^{C} can be calculated from Eq. 6:

$$T_1^{\mathrm{C}} = \frac{g_{T1}}{\beta_1 g_1}(T_1^0 - T_1^{\mathrm{F}}) \qquad T_2^{\mathrm{C}} = \frac{g_{T2}}{\beta_2 g_2}(T_2^0 - T_2^{\mathrm{F}}) \quad [18]$$

and can be simplified using Eq. 17:

$$T_1^{\mathrm{C}} \simeq \begin{cases} \dfrac{g_{T1}}{g_1 \beta_1} T_1^0 & , \text{if } T_1^0 + \phi_{21} < \theta_1 \\ \dfrac{g_{T1}}{g_1 \beta_1}(\theta_1 - \dfrac{\alpha_2 g_2 \beta_1}{\alpha_1 g_{T1}} T_2^{\mathrm{C}}) & , \text{if } T_1^0 + \phi_{21} > \theta_1 \end{cases} \quad [19]$$

The turning point in Eqs. 17 and 19:

$$T_1^0 + \phi_{21} = \theta_1 \quad [20]$$

can be regarded as a threshold to distinguish regimes of the system: "R abundant" ($T_1^0 + \phi_{21} \ll \theta_1$), "$R$ equimolar" ($T_1^0 + \phi_{21} \simeq \theta_1$) and "$R$ scarce" ($T_1^0 + \phi_{21} \gg \theta_1$). Eqs. 17 and 19 explain why the relationships between competitors are piecewise (Figure 2A-C). For T_1^{F} and T_2^{F}, according to Eq. 17, in "R abundant" regime ($T_1^0 + \phi_{21} \ll \theta_1$), almost all targets bind with R, so the level of T_1^{F} approaches to zero. In the contrary, in "R scarce" regime ($T_1^0 + \phi_{21} \gg \theta_1$), T_1^{F} increases with

the increment of T_2^{F}, which is because when the production rate of T_2 raises to sequester R, T_2^{C} increases thus $T_2^0 - T_2^{\mathrm{F}}$ increases according to Eq. 18. Given the above, when the production rate of T_2 increases to switch the system from R "abundant" regime to "R scarce" regime, the abundance of T_1^{F} will exhibit a "threshold behavior" (Figure 2B).

Similarly, Eq. 19 suggested that the relationship between T_1^{C} and T_2^{C} is piecewise linear. If R is abundant ($T_1^0 + \phi_{21} \ll \theta_1$), T_1^{C} would keep substantially unchanged, while when R is scarce ($T_1^0 + \phi_{21} \gg \theta_1$), T_1^{C} would decrease linearly with the increment of T_2^{C}, thus shows "negative linear dependence" (Figure 2C).

2.3. Approximation of the regime threshold. The threshold (Eq. 20) can be approximated based on the strong binding assumption. It is equivalent to:

$$\frac{k_{T1}}{g_{T1}} + \frac{\alpha_2\beta_1 g_{T2}}{\alpha_1\beta_2 g_{T1}}\left(\frac{k_{T2}}{g_{T2}} - T_2^{\mathrm{F}}\right) = \frac{\beta_1 k_R}{\alpha_1 g_{T1}} \quad [21]$$

From Eq. 3, we get

$$T_1^{\mathrm{F}} = \frac{k_{1-} + g_1}{R^{\mathrm{F}} k_{1+}} T_1^{\mathrm{C}} \quad [22]$$

According to Eq. 17, before the system reaches the threshold ($T_1^0 + \phi_{21} \leq \theta_1$) in the process of increment of production of T_2, T_1^{F} is much smaller than T_1^{C} and approaches to zero, and so does T_2^{F}. Thus, the threshold point ($T_1^0 + \phi_{21} = \theta_1$) could be approximated from Eq. 21 as:

$$\frac{\alpha_1}{\beta_1} k_{T1} + \frac{\alpha_2}{\beta_2} k_{T2} = k_R \quad [23]$$

Eq. 23 gives an approximation of the threshold position to estimate the regime of a competing system roughly.

3. Competition can shape the regulator-target response curve.

3.1. How competition shapes regulator-target response curve. According to Eq. 9, there are

$$F(k_R, T_1^{\mathrm{F}}, T_2^{\mathrm{F}}) = (T_1^{\mathrm{F}})^2 - T_1^{\mathrm{F}}(T_1^0 - \lambda_1 - \theta_1 + \phi_{21}) - \lambda_1 T_1^0 = 0 \quad [24]$$

$$G(k_R, T_1^{\mathrm{F}}, T_2^{\mathrm{F}}) = (T_2^{\mathrm{F}})^2 - T_2^{\mathrm{F}}(T_2^0 - \lambda_2 - \theta_2 + \phi_{12}) - \lambda_2 T_2^0 = 0 \quad [25]$$

Thus,

$$\frac{\partial T_1^{\mathrm{F}}}{\partial k_R} = \frac{\begin{vmatrix} \frac{\partial F}{\partial k_R} & \frac{\partial F}{\partial T_2^{\mathrm{F}}} \\ \frac{\partial G}{\partial k_R} & \frac{\partial G}{\partial T_2^{\mathrm{F}}} \end{vmatrix}}{\begin{vmatrix} \frac{\partial F}{\partial T_1^{\mathrm{F}}} & \frac{\partial F}{\partial T_2^{\mathrm{F}}} \\ \frac{\partial G}{\partial T_1^{\mathrm{F}}} & \frac{\partial G}{\partial T_2^{\mathrm{F}}} \end{vmatrix}} = -\frac{\gamma_1}{1 + \frac{\lambda_1 T_1^0}{\lambda_2 T_2^0}(\frac{T_2^{\mathrm{F}}}{T_1^{\mathrm{F}}})^2 + \frac{\lambda_1 T_1^0}{(T_1^{\mathrm{F}})^2}} \quad [26]$$

$$\frac{\partial \log T_1^{\mathrm{F}}}{\partial \log k_R} = \frac{k_R}{T_1^{\mathrm{F}}}\frac{\partial T_1^{\mathrm{F}}}{\partial k_R} = -\frac{\gamma_1 k_R}{T_1^{\mathrm{F}} + \frac{\lambda_1 T_1^0}{\lambda_2 T_2^0}\frac{(T_2^{\mathrm{F}})^2}{T_1^{\mathrm{F}}} + \frac{\lambda_1 T_1^0}{T_1^{\mathrm{F}}}} \quad [27]$$

Eq. 27 describes the derivative of regulator-target response curve (Figure 2E and 2G).

Similarly, the buffer capacity, which quantifies the ability to resist pH changes in buffer solution, can be calculated as

$$B = -\frac{\partial k_R}{\partial \log T_1^{\mathrm{F}}} = \frac{1}{\gamma_1}(T_1^{\mathrm{F}} + \frac{\lambda_1 T_1^0}{\lambda_2 T_2^0}\frac{(T_2^{\mathrm{F}})^2}{T_1^{\mathrm{F}}} + \frac{\lambda_1 T_1^0}{T_1^{\mathrm{F}}}) \quad [28]$$

3.2. Competition in buffer solution. For any buffer solution with a weak acid (HA) and its conjugate base (A^-) or a weak base (BOH) and its conjugate acid (B^+), there are

$$H_2O \rightleftharpoons H^+ + OH^-$$

$$HA \rightleftharpoons H^+ + A^-$$

$$BOH \rightleftharpoons B^+ + OH^-$$

Here we take ammonium buffer solution ($NH_3 \cdot H_2O$ and NH_4Cl) as an example. In a aqueous solution with a mol/L $NH_3 \cdot H_2O$ and b mol/L NH_4Cl, there are

$$H_2O \rightleftharpoons H^+ + OH^-$$

$$NH_3 \cdot H_2O \rightleftharpoons {NH_4}^+ + OH^-$$

The equilibrium constants of these two reactions are

$$K_1 = \frac{[H^+][OH^-]}{[H_2O]} \quad [29]$$

$$K_2 = \frac{[{NH_4}^+][OH^-]}{[NH_3 \cdot H_2O]} \quad [30]$$

Because the concertation water of in an aqueous solution is almost invariant, the equilibrium constant of water (ion-product constant) is defined as

$$K_{\mathrm{w}} = [H^+][OH^-] = K_1[H_2O] \simeq 10^{-14}\,\mathrm{mol} \cdot \mathrm{L}$$

Here, we consider H^+ (T_1) and $NH_4{}^+$ (T_2) competing for OH^- (R). Thus, Eqs. 29 and 30 is equivalent to

$$K_1 = \frac{T_1^{\mathrm{F}} R^{\mathrm{F}}}{T_1^{\mathrm{C}}} \quad [31]$$

$$K_2 = \frac{T_2^{\mathrm{F}} R^{\mathrm{F}}}{T_2^{\mathrm{C}}} \quad [32]$$

Meanwhile, because there are no production and degradation of any component, every substance is conserved as

$$T_1^{\mathrm{F}} + T_1^{\mathrm{C}} = T_1^{\mathrm{A}} = w \quad [33]$$

$$T_2^{\mathrm{F}} + T_2^{\mathrm{C}} = T_2^{\mathrm{A}} = a + b \quad [34]$$

$$T_1^{\mathrm{C}} + T_2^{\mathrm{C}} + R^{\mathrm{F}} = R^{\mathrm{A}} = a + w \quad [35]$$

Combining Eqs. 33-35, we get

$$R^{\mathrm{F}} = R^{\mathrm{A}} - T_1^{\mathrm{A}} - T_2^{\mathrm{A}} + T_1^{\mathrm{F}} + T_2^{\mathrm{F}} \quad [36]$$

Combining Eqs. 31, 32 and 36, we get

$$T_1^{\mathrm{F}} = \frac{1}{2}(T_1^{\mathrm{A}} + T_2^{\mathrm{A}} - R^{\mathrm{A}} - T_2^{\mathrm{F}} - K_1 + \sqrt{(T_1^{\mathrm{A}} + T_2^{\mathrm{A}} - R^{\mathrm{A}} - T_2^{\mathrm{F}} - K_1)^2 + 4K_1 T_1^0}) \quad [37]$$

which is a degenerate form of Eq. 15, where

$$\alpha_1 = \alpha_2 = \beta_1 = \beta_2 \qquad g_{T1} = g_{T2}$$

$$K_1 = \frac{g_R}{\alpha_1 k_{1+}}(\frac{k_{1-}}{g_1} + 1) \qquad K_2 = \frac{g_R}{\alpha_2 k_{2+}}(\frac{k_{2-}}{g_2} + 1)$$

$$T_1^{\mathrm{A}} = k_{T1}/g_{T1} \qquad T_2^{\mathrm{A}} = k_{T2}/g_{T2}$$

$$R^{\mathrm{A}} = k_R/g_{T1} = k_R/g_{T2}$$

According to Eq. 28, the buffer capacity of this solution is

$$B = \frac{\partial R}{\partial \mathrm{pOH}} = T_1^{\mathrm{F}} + \frac{K_{\mathrm{w}}}{K_2 T_2^{\mathrm{A}}}\frac{(T_2^{\mathrm{F}})^2}{T_1^{\mathrm{F}}} + \frac{K_{\mathrm{w}}}{T_1^{\mathrm{F}}} = [\mathrm{OH}^-] + \frac{K_2(a+b)[\mathrm{OH}^-]}{(K_2 + [\mathrm{OH}^-])^2} + [\mathrm{H}^+] \quad [38]$$

Eq. 38 indicates that when a mild change of OH^- is introduced to the solution, the buffer capacity guarantees the stable of pOH (and pH). More buffer substance ($NH_4{}^+$ and $NH_3 \cdot H_2O$, $a + b$) can lead to a larger buffer capacity, and the buffer capacity may maximize when $\mathrm{pH} = \mathrm{p}K_2$.

3.3. Dose-response curve of free target to free regulator. Substituting Eq. 22 into Eq. 2, we get

$$k_{T1} - T_1^{\mathrm{F}} g_{T1} - k_{1+} R^{\mathrm{F}} T_1^{\mathrm{F}} + (k_{1-} + (1-\beta_1) g_1) T_1^{\mathrm{C}} = 0 \quad [39]$$

Thus,

$$\frac{T_1^{\mathrm{F}}}{T_1^0} = \frac{1}{1 + O_1 R^{\mathrm{F}}}, \text{ where } O_1 = \frac{\beta_1 k_{1+}}{g_{T1}(1 + \frac{k_{1-}}{g_1})} \quad [40]$$

In system with n targets competing for same regulator, for the ith target ($i = 1,\ 2,\ \cdots,\ n$), this result can be extended as:

$$\frac{T_i^{\mathrm{F}}}{T_i^0} = \frac{1}{1 + O_i R^{\mathrm{F}}}, \text{ where } O_i = \frac{\beta_i k_{i+}}{g_{Ti}(1 + \frac{k_{i-}}{g_i})} \quad [41]$$

Similarly,

$$\frac{T_i^{\mathrm{C}}}{T_i^0} = \frac{g_{Ti}}{\beta_i g_i}(1 - \frac{1}{1 + O_i R^{\mathrm{F}}}) \quad [42]$$

Eqs. 41 and 42 indicate that the level of T_i^{F} and T_i^{C} are determined only by the free level of R, and some chemical kinetic parameters of T_i and R. In another wordsif two or more tagets compete for shared R, the relative abundances of each free target or complex are independent of other targets when giving the free level of R. In the siRNA design strategy (Yuan et al., 2015; Yuan et al., 2016),this property guarantees that no matter what expression of the off-target gene is (unless the expression is zero), the amount of free siRNA required to repress the target gene to a certain extent would always repress the off-target gene to a certain extent, which is determined by O_{on} and O_{off}, as described in Eq. 41. When giving the expression of any target gene, siRNA could act as a medium to predict the expression of other target genes. This property also guides how to select suitable chemical reaction parameters: a good siRNA should have large O_{on} and small O_{off}.

4. Competition can delay or accelerate dynamic response.

When R level changes, comparisons of $\frac{\mathrm{d}\,R^{\mathrm{F}}}{\mathrm{d}\,t}$ tells how competition affects the dynamic response speed of T_1 with respect to R. According to Eq. 1 and 5,

$$\begin{aligned}\frac{\mathrm{d}\,R^{\mathrm{F}}}{\mathrm{d}\,t} =& k_R - g_R R^{\mathrm{F}} - k_{1+} T_1^{\mathrm{F}} R^{\mathrm{F}} + k_{1-} T_1^{\mathrm{C}} + (1-\alpha_1) g_1 T_1^{\mathrm{C}} \\ & \underbrace{-k_{2+} T_2^{\mathrm{F}} R^{\mathrm{F}} + k_{2-} T_2^{\mathrm{C}} + g_2 T_2^{\mathrm{C}}}_{\mathrm{A}} \ \underbrace{-\alpha_2 g_2 T_2^{\mathrm{C}}}_{\mathrm{B}}\end{aligned} \quad [43]$$

Item A equals to $-\frac{\mathrm{d}\,T_2^{\mathrm{C}}}{\mathrm{d}\,t}$, and indicates the ability of T_2 to sequester R when T_2^{C} forms ($-\frac{\mathrm{d}\,T_2^{\mathrm{C}}}{\mathrm{d}\,t} < 0$), or release R when T_2^{C} dissociates ($-\frac{\mathrm{d}\,T_2^{\mathrm{C}}}{\mathrm{d}\,t} > 0$). Item B indicates the level of R loss mediated by T_2^{C} degradation.

On the rising edge of R, T_2^{C} forms so item A < 0, meanwhile item B < 0 all the time, thus $\frac{\mathrm{d}\,R^{\mathrm{F}}}{\mathrm{d}\,t}$ is smaller than non-competing system, leading to a slower response. On the falling edge of R, item A > 0 while item B < 0, thus the response speed depends on the relative magnitude of item A and B. As g_2 or α_2 increases, the absolute value of item B increases to alter the response from delay to acceleration. As k_2^+ increases or k_2^- decreases, item A increases while the absolute value of item B also increases because T_2^{C} becomes larger, thus delay the response when there is no R loss mediated by T_2^{C} ($g_2 = 0$, Figure S3D), alter the response from delay to acceleration when g_2 is moderate (Figure S3E), or accelerate the response when g_2 is large enough (Figure S3F).

5. Noise and correlated flucuation evaluation.

The variances and co-variances of the molecular species in the system can be estimated with linear noise approximation. Fluctuation-dissipation theorem provides a general way to quantifies the fluctuations. The fluctuation-dissipation equation was solved numerically to calculate the covariance matrix $\boldsymbol{C}$, the diagonal elements of which are the variance of corresponding entities, while the off-diagonal elements of which describe the co-variances between molecular species. The noise of a molecular species i is defined as coefficient of variation $\sigma(x_i)/\bar{x_i}$ and the correlation between two molecular species i and j is defined as $\mathrm{cov}(x, y)/(\sigma(x_i)\sigma(x_j))$, where x_i and x_j are random variables representing the abundance of molecular species i and j.

Taking miRNA competing system as an example (where miRNA acts as repressor), the vector of molecular number

$$\boldsymbol{N} = \begin{bmatrix} R^{\mathrm{F}} & T_1^{\mathrm{F}} & T_2^{\mathrm{F}} & T_1^{\mathrm{C}} & T_2^{\mathrm{C}} & P_1 & P_2 \end{bmatrix} \tag{44}$$

Transition rates vector is

$$\begin{aligned} \boldsymbol{f}(\boldsymbol{x}) = \Big[\;& k_{T1} \quad g_{T1}T_1^{\mathrm{F}} \quad k_{1+}T_1^{\mathrm{F}}R^{\mathrm{F}} \quad k_{1-}T_1^{\mathrm{C}} \quad g_1\,(1-\beta_1)\,T_1^{\mathrm{C}} \quad k_{T2} \quad g_{T2}T_2^{\mathrm{F}} \\ & k_{2+}T_2^{\mathrm{F}}R^{\mathrm{F}} \quad k_{2-}T_2^{\mathrm{C}} \quad g_2\,(1-\beta_2)\,T_2^{\mathrm{C}} \quad k_R \quad g_R R^{\mathrm{F}} \quad g_1\,(1-\alpha_1)\,T_1^{\mathrm{C}} \\ & g_1\,(\alpha_1+\beta_1-1)\,T_1^{\mathrm{C}} \quad g_2\,(1-\alpha_2)\,T_2^{\mathrm{C}} \quad g_2\,(\alpha_2+\beta_2-1)\,T_2^{\mathrm{C}} \quad k_{P1}T_1^{\mathrm{F}} \\ & g_{P1}P_1 \quad k_{P2}T_2^{\mathrm{F}} \quad g_{P2}P_2 \Big] \end{aligned} \tag{45}$$

Stoichiometric matrix is

$$\boldsymbol{S} = \begin{bmatrix} 1 & -1 & -1 & 1 & 1 & 0 & 0 & 0 & 0 & 0 & 0 & 0 & 0 & 0 & 0 & 0 & 0 & 0 & 0 & 0 \\ 0 & 0 & 0 & 0 & 0 & 1 & -1 & -1 & 1 & 1 & 0 & 0 & 0 & 0 & 0 & 0 & 0 & 0 & 0 & 0 \\ 0 & 0 & -1 & 1 & 0 & 0 & 0 & -1 & 1 & 0 & 1 & -1 & 1 & 1 & 0 & 0 & 0 & 0 & 0 & 0 \\ 0 & 0 & 1 & -1 & -1 & 0 & 0 & 0 & 0 & 0 & 0 & 0 & -1 & 0 & -1 & 0 & 0 & 0 & 0 & 0 \\ 0 & 0 & 0 & 0 & 0 & 0 & 0 & 1 & -1 & -1 & 0 & 0 & 0 & -1 & 0 & -1 & 0 & 0 & 0 & 0 \\ 0 & 0 & 0 & 0 & 0 & 0 & 0 & 0 & 0 & 0 & 0 & 0 & 0 & 0 & 0 & 0 & 1 & -1 & 0 & 0 \\ 0 & 0 & 0 & 0 & 0 & 0 & 0 & 0 & 0 & 0 & 0 & 0 & 0 & 0 & 0 & 0 & 0 & 0 & 1 & -1 \end{bmatrix} \quad [46]$$

In the steady state, the rate equations can be linearized by the Jacobian matrix:

$$\boldsymbol{J} = \boldsymbol{S} \cdot \frac{\partial \boldsymbol{f}(\boldsymbol{x})}{\partial \boldsymbol{N}} \quad [47]$$

The diffusion matrix $\boldsymbol{D}$ is

$$\boldsymbol{D} = \boldsymbol{S} \cdot \mathrm{diag}(\boldsymbol{f}(\boldsymbol{x})) \cdot \boldsymbol{S}^{\top} \quad [48]$$

Therefore, the covariance matrix $\boldsymbol{C}$ can be calculate numerically by solving the fluctuation dissipation equation:

$$\boldsymbol{J} \cdot \boldsymbol{C} + \boldsymbol{C} \cdot \boldsymbol{J}^{\top} + \boldsymbol{D} = \boldsymbol{0} \quad [49]$$

6. Regulator allocation to multiple targets.

When there are n targets, similarly to Eqs. 1-5, there are

$$\frac{\mathrm{d}\,R^{\mathrm{F}}}{\mathrm{d}\,t} = k_R - g_R R^{\mathrm{F}} + \sum_{i=1}^{n}(-k_{i+} T_i^{\mathrm{F}} R^{\mathrm{F}} + k_{i-} T_i^{\mathrm{C}} + (1-\alpha_i) g_i T_i^{\mathrm{C}}) \quad [50]$$

$$\frac{\mathrm{d}\,T_i^{\mathrm{F}}}{\mathrm{d}\,t} = k_{Ti} - g_{Ti} T_i^{\mathrm{F}} - k_{i+} T_i^{\mathrm{F}} R^{\mathrm{F}} + k_{i-} T_i^{\mathrm{C}} + (1-\beta_i) g_i T_i^{\mathrm{C}} \quad [51]$$

$$\frac{\mathrm{d}\,T_i^{\mathrm{C}}}{\mathrm{d}\,t} = k_{i+} T_i^{\mathrm{F}} R^{\mathrm{F}} - k_{i-} T_i^{\mathrm{C}} - g_i T_i^{\mathrm{C}} \quad [52]$$

At steady states, by adding Eqs. 50 and 52, we get

$$R^{\mathrm{F}} = \frac{k_R - \sum_i \alpha_i T_i^{\mathrm{C}} g_i}{g_R} \quad [53]$$

Solving Eq. 52, we get

$$T_i^{\mathrm{F}} = \frac{k_{i-} + g_i}{R^{\mathrm{F}} k_{i+}} T_i^{\mathrm{C}} \quad [54]$$

Combining Eqs. 53 and 54, we get

$$R^{\mathrm{F}} = \frac{k_R}{g_R + \sum_i Q_i} \quad [55]$$

where

$$Q_i = \alpha_i g_i \frac{k_{i+}}{k_{i-} + g_i} T_i^{\mathrm{F}} \quad [56]$$

Thus,

$$\alpha_i g_i T_i^{\mathrm{C}} = \frac{Q_i}{g_R + \sum_j Q_j} k_R \quad [57]$$

Eq. 57 has the exact form of current divider rule in electronics:

$$I_i = \frac{\frac{1}{R_i}}{\frac{1}{R_0} + \sum_j \frac{1}{R_j}} I_{\mathrm{total}} \quad [58]$$

It inspires that R's production rate (k_R) is analogous to the total current (I_{total}); the capability of T_i^{C} to consume R ($\alpha_i g_i T_i^{C}$) is analogous to the ith branch current (I_i); and the capability of T_i^{F} to occupy R (Q_i) is analogous to the ith branch conductance ($1/R_i$).

When R is scarce, $T_i^{\mathrm{F}} \simeq T_i^0$, thus Eq. 56 is approximated to

$$Q_i \simeq \alpha_i g_i \frac{k_{i+}}{k_{i-} + g_i} T_i^0 \quad [59]$$

which indicates that in the "R scarce" regime, the capability of T_i to occupy R (resistance) is only determined by the parameter settings of T_i.

For catalytic reactions with a constat level of enzyme (regulator) and substances (targets), Eqs. 50-52 degenerate as

$$\frac{\mathrm{d}\, R^{\mathrm{F}}}{\mathrm{d}\, t} = \sum_{i=1}^{n} (-k_{i+} T_i^{\mathrm{F}} R^{\mathrm{F}} + k_{i-} T_i^{\mathrm{C}} + g_i T_i^{\mathrm{C}}) \quad [60]$$

$$\frac{\mathrm{d}\, T_i^{\mathrm{F}}}{\mathrm{d}\, t} = -k_{i+} T_i^{\mathrm{F}} R^{\mathrm{F}} + k_{i-} T_i^{\mathrm{C}} \quad [61]$$

$$\frac{\mathrm{d}\, T_i^{\mathrm{C}}}{\mathrm{d}\, t} = k_{i+} T_i^{\mathrm{F}} R^{\mathrm{F}} - k_{i-} T_i^{\mathrm{C}} - g_i T_i^{\mathrm{C}} \quad [62]$$

Under the assumption of Michaelis-Menten kinetics that $\frac{\mathrm{d}\, T_i^{\mathrm{C}}}{\mathrm{d}\, t} = 0$, define $K_i = (k_{i-} + g_i)/k_{i+}$, then we get

$$T_i^{\mathrm{C}} = \frac{T_i^{\mathrm{F}}}{K_i} R^{\mathrm{F}} \quad [63]$$

Thus,

$$R^{\mathrm{total}} = R^{\mathrm{F}} + \sum_j T_j^{\mathrm{C}} = R^{\mathrm{F}} (1 + \sum_j T_j^{\mathrm{F}} / K_j) \quad [64]$$

$$R^{\mathrm{F}} = \frac{1}{1 + \sum_j T_i^{\mathrm{F}} / K_i} R^{\mathrm{total}} \quad [65]$$

$$T_i^{\mathrm{C}} = \frac{T_i^{\mathrm{F}} / K_i}{1 + \sum_j T_j^{\mathrm{F}} / K_j} R^{\mathrm{total}} \quad [66]$$

Which is the formation of enzyme allocation in Michaelis-Menten kinetics systems (Chou and Talaly, 1977).

7. Simulation parameters for drawing figures.

The scales of simulation parameters are referenced from previous publications across different competition scenarios, such as transcription (Jayanthi et al., 2013), post-transcription (Ala et al., 2013; Schmiedel et al., 2015),translation (Gorochowski et al., 2016),degradation (Cookson et al., 2011)and chemical buffer solutions. Table S1 lists the parameters for drawing figures, the scales of which are derived from from previous researches on ceRNA effects (Ala et al., 2013; Yuan et al., 2015; Yuan et al., 2016)All gradually changing parameters are shown in figures. In Figure 2F-G and S2D-E, $k_{T2} = 1 \times 10^{-2}$. In Figure 2I, $k_{T2} = 1 \times 10^{-4}$, and parameters of T_3 are shown in Table S1. In Figure 3A-C and S3A-F, $g_1 = 4 \times 10^{-5}$, $k_{T2} = 1 \times 10^{-4}$. In Figure S3A, $g_2 = 3.2 \times 10^{-4}$. In Figure 3E-H, for dashed blue lines, $k_R = 5 \times 10^{-3}$; for thick blue lines, $k_R = 7.81 \times 10^{-5}$; for thick green lines, $k_R = 5 \times 10^{-3}$, $k_{T2} = 3.21 \times 10^{-2}$. In Figure S3G-J, $k_{T1} = 5 \times 10^{-3}$.

Table S1. Primary parameters for simulations

Primary parameters						Additional parameters for Figure 2I	
R		T_1		T_2		T_3	
k_R	5×10^{-3}	k_{T1}	1×10^{-3}	k_{T2}	8×10^{-3}	k_{T3}	5×10^{-4}
g_R	1×10^{-4}	g_{T1}	1×10^{-5}	g_{T2}	1×10^{-5}	g_{T3}	1×10^{-5}
		k_{1+}	1×10^{-4}	k_{2+}	1×10^{-4}	k_{3+}	1×10^{-6}
		k_{1-}	5×10^{-5}	k_{2-}	5×10^{-5}	k_{3-}	5×10^{-5}
		g_1	8×10^{-5}	g_2	8×10^{-5}	g_3	1×10^{-5}
		α_1	1	α_2	0.5	α_3	0.5
		β_1	1	β_2	1	β_3	1
		k_{P1}	1×10^{-2}				
		g_{P1}	5×10^{-6}				

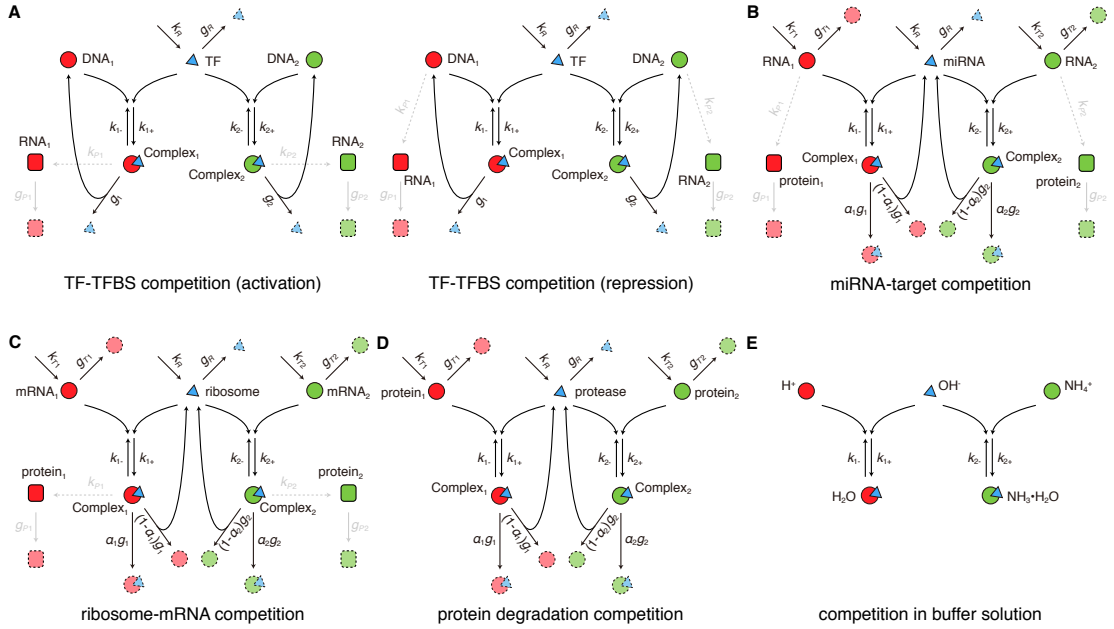

Figure S1 Detailed descriptions under the unified coarse-gained competition motif model for diverse competition scenarios.

(A) DNA TF binding sites (TFBS) competing for TFs. Left: TF acts as an activator; right: TF acts as a repressor.

(B) RNA molecules competing for miRNAs.

(C) RNA molecules competing for ribosomes.

(D) Proteins competing for proteases.

(E) Competition in the ammonium buffer solution, where H^+ and NH_4^+ compete for OH^-.

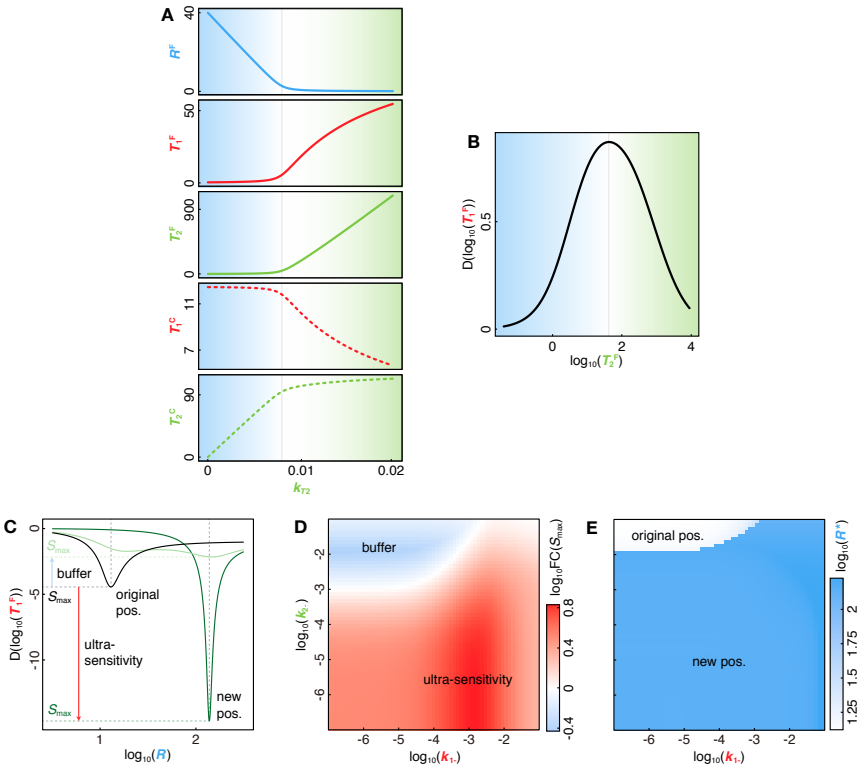

Figure S2 Steady state behaviors of competition systems.

(A) Abundances of each component in Figure 2A on linear scales.

(B) Derivatives of the curve in Figure 2B. Each component's abundance in competition motif changing with T_2's production rate (k_{T2}). Colors, lines and parameter settings are the same with Figure 2A-C.

(C) Schematic diagram depicting the maximum sensitivity (S_{max}) and its position (R^*) of R-T_1 dose-response curves. Dose-response curves are adopted from Figure 3G.

(D-E) Relative binding affinities of T_1 and T_2 (k_{1-} and k_{2-}) shape R-T_1 dose-response curves. (D) Fold change of S_{max} compared with that of non-competing system (k_{T2}=0). Competition of T_2 buffers the response of T_1^F to R when $\log_{10}FC(S_{max})<0$, but introduces larger sensitivity when $\log_{10}FC(S_{max})>0$. (E) Changes of R^*.

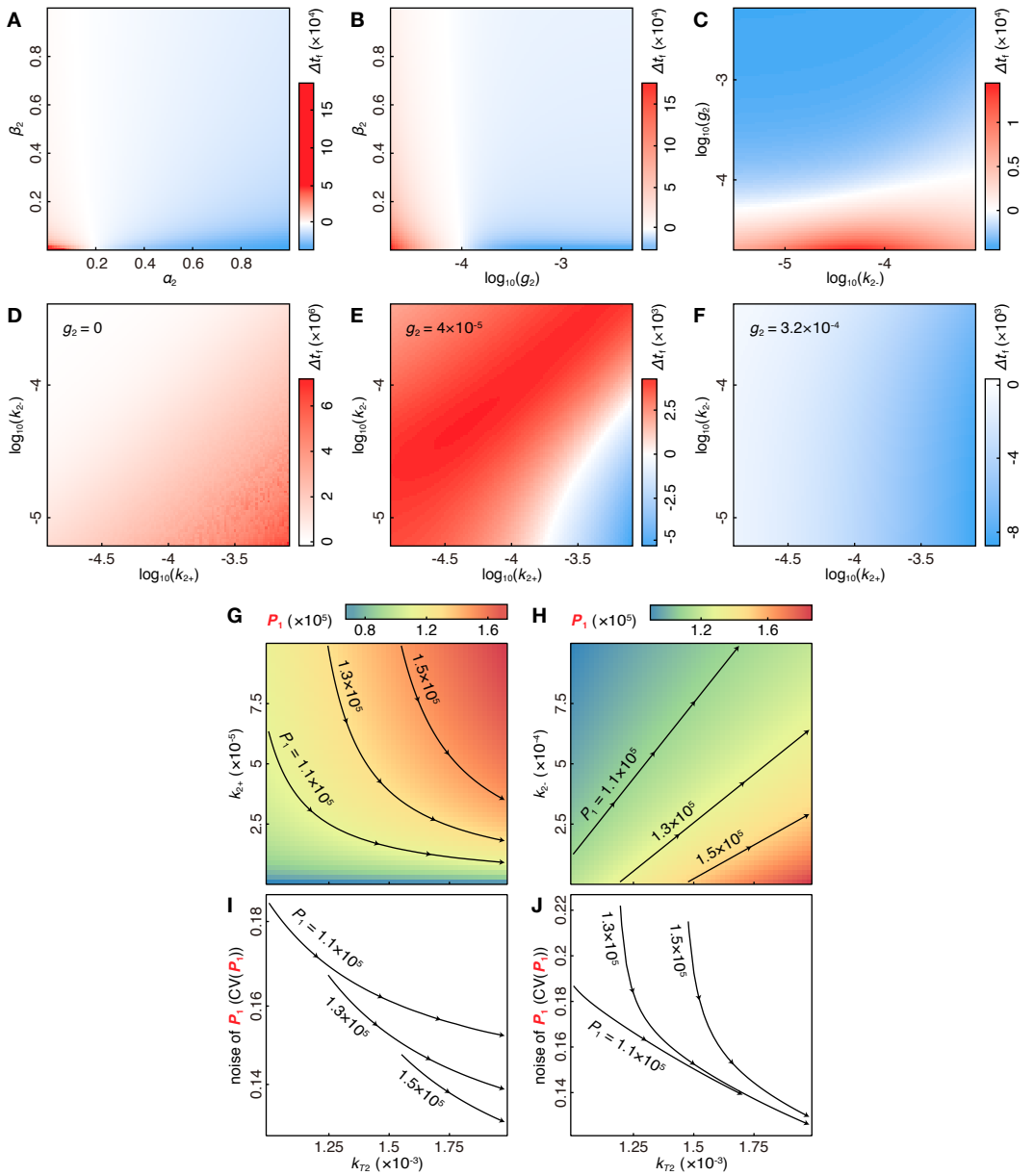

Figure S3 Dynamic properties of competition systems.

(A-F) Modifications of response time on the falling edge of *R*'s change under different kinetic parameters: (A) different α_2 and β_2; (B) different g_2 and β_2; (C) different k_{2-} and g_2; (D-F) different k_{2+}, k_{2-} and g_2 (values of g_2 are shown in figures).

(G-J) Abundant weak competitors can buffer target expression noise better. (G-H) P_1 level changing with T_2's production rate (k_{T2}) and T_2's association rate (k_{2+}) (G), or k_{T2} and T_2's dissociation rate (k_{2-}) (H). Black lines are T_1^F level isolines. (I-J) Target expression noise changes on the isolines in (G) and (H) respectively. Along the direction of the arrows, T_2's production increases and T_2's binding affinity decreases, bringing about lower expression noise.